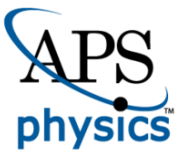

Competing Kinetics and He Bubble Morphology in W

Luis Sandoval, Danny Perez, Blas P. Uberuaga, and Arthur F. Voter

Phys. Rev. Lett. **114**, 105502 — Published 11 March 2015

DOI: 10.1103/PhysRevLett.114.105502

Competing kinetics and He bubble morphology in W

Luis Sandoval,[1] Danny Perez,[1] Blas P. Uberuaga,[2] and Arthur F. Voter[1]

[1] *Theoretical Division, Los Alamos National Laboratory, Los Alamos, NM 87545, USA*
[2] *Materials Science and Technology Division, Los Alamos National Laboratory, Los Alamos, NM 87545 USA*

The growth process of He bubbles in W is investigated using molecular dynamics and parallel replica dynamics for growth rates spanning six orders of magnitude. Fast and slow growth regimes are defined relative to typical diffusion hopping times of W interstitials around the He bubble. Slow growth rates allow the diffusion of interstitials around the bubble, favoring the biased growth of the bubble towards the surface. In contrast, at fast growth rates interstitials do not have time to diffuse around the bubble, leading to a more isotropic growth and increasing the surface damage.

One of the most important challenges for the successful commercialization of fusion power is the development of plasma facing materials (PFMs) [1, 2] that can tolerate the extreme conditions of elevated temperatures and high particle flux of H isotopes and He present in fusion reactors. W is an attractive material for such applications, mainly due to its low hydrogen solubility, low sputtering yield, high melting point, and high thermal conductivity [3]. However, the material is still deleteriously affected by the plasma and fusion byproducts. In particular, the He irradiation modifies the near-surface microstructure by creating bubbles [4]. This is a key problem, as He bubbles increase the retention of tritium in the wall, drastically influencing the long-term thermo-mechanical stability and creating a large radioactive inventory, with hazardous consequences and significant increase in fuel costs. Moreover, experiments have shown that a fuzz-like nanostructure develops on the W surface under the operating conditions (temperature, He impact energy, and He flux) expected for ITER's divertor, which increases the nucleation of bubbles, the retention of hydrogen isotopes, and the production of high-Z dust [5, 6].

While numerous computational studies have examined He-W interactions [7–14], these correspond to unrealistically high He uptake scenarios as compared to typical experimental conditions [15]. The impact of such high rates on the microstructural evolution is unclear. As detailed below, we find that access to dynamics on longer time scales, which approach experimentally relevant conditions, significantly improves our physical understanding of the growth process for He bubbles, in particular the role of interstitial diffusion around the bubbles, which is very limited on direct molecular dynamics (MD) time scales. Specifically, we find that the competing kinetics of growth of the bubbles and of diffusion of interstitials around the bubbles significantly impact their evolution and morphology because it affects the ability of the system to equilibrate with respect to the bias created by neighboring microstructural features such as the W surface.

In this work, we report a study across time scales of He bubble growth in W using MD and parallel replica dynamics (ParRep) [16, 17]. ParRep enables the temporal parallelization of the state-to-state dynamics hence allowing massively parallel resources to be leveraged in order to reach very long simulation timescales on systems of modest sizes. For example, some of our results were generated using 10000 replicas distributed over 160000 cores on the Titan supercomputer at Oak Ridge National Laboratory. This enables the investigation of the growth process of a single He bubble at growth rates spanning six orders of magnitude, from $10^{12} - 2\times10^{6}\,\mathrm{He\,s^{-1}}$, corresponding to simulation times ranging between 0.3 ns and 3 μs, approximately. In contrast, typical MD simulations are carried out at rates of around $10^{11}\,\mathrm{He\,s^{-1}}$ for a few ns. ParRep therefore allows one to reach a qualitatively different growth regime that is inaccessible to standard MD simulations.

Our simulation box contains 16399 W atoms arranged on a bcc lattice with dimensions $20a \times 20.5a \times 20a$, with $a = 3.183$ Å, the lattice constant of W at 1000 K. Temperature is controlled using a Langevin thermostat applied on the bottom-most $4a$ of the box, while the rest of the atoms evolves in the microcanonical ensemble. Periodic boundary conditions are defined only in two directions, and the W surface is parallel to the (100) plane. MD and ParRep simulations are performed with the open source code LAMMPS [18]. The interaction between W atoms is determined by an Ackland-Thetford potential [19], modified at short distances by Juslin and Wirth [11]. He-W interactions were obtained from Juslin and Wirth [11, 20], while the He-He potential corresponds to the one used by Beck [21] modified at short distances by Morishita et al [22].

The growth of a single He bubble is controlled by directly inserting He atoms into the bubble at constant time intervals. In reality, this process would occur following the absorption of isolated He atoms or small He clusters (< 8 atoms [23]) that encounter the bubble as they diffuse in the W bulk. This growth rate can be associated to an impinging He flux by considering the fraction of incoming ions that reach the bubble [20]. The slowest growth rate considered in this work corresponds to a flux of approximately $1.2 \times 10^{24}\,\mathrm{He\,m^{-2}\,s^{-1}}$, which is on the order of magnitude expected at ITER [24]. An initial bubble is created by placing eight He atoms inside

a pre-existing W vacancy. This choice is justified by the observation that, once an interstitial He cluster has accumulated $\gtrsim 5$ He atoms, it is able to create a W Frenkel pair [23], the so-called *self-trapping* process, after which the bubble is practically immobile on the timescales considered here. The initial vacancy is located at a depth of $6a = 1.91$ nm, based on our observation of bubble formation in a direct MD simulation [20].

It is known from direct MD simulations [13] that successive addition of He atoms in the bubble increases the pressure, which is the driving force for nucleation of additional Frenkel pairs. Each formation of one or more Frenkel pairs partially releases the pressure experienced by the bubble and increases the bubble size. As growth progresses, the corresponding interstitials aggregate into prismatic $\langle 111 \rangle$ dislocation loops that are ultimately emitted from the bubble to form adatom islands on the surface [25]. The process continues until the bubble comes within a few layers of the surface, at which point it bursts, creating a crater or a pinhole.

We first consider the growth rate effects at the beginning of the He bubble growth process. The bubble He content after the first *trap mutation* event, in which a W atom is pushed out of the surface of the bubble, creating an additional vacancy (leaving the system with two W vacancies and one W interstitial), strongly depends on the growth rate, as shown in Fig. 1(a). Slowing the growth process by six orders of magnitude decreases the number of He atoms at which this transition is triggered by almost 50%. This is a reflection of the interplay between the He insertion rate and the Frenkel pair nucleation rate, as at fast insertion the probability of creating a new Frenkel pair before the next He insertion is small. As the growth rate is lowered, this probability increases, leading to smaller He-to-vacancy ratios, and hence lower pressures, c.f. Fig. 1(b).

Other structural consequences of the growth rate are presented in Fig. 1(c-e). From Panels c) and d) it is apparent that slow growth rates favor growth that is more directed towards the surface compared to fast growth rates. Indeed, the center of mass of the bubble moves towards the surface faster at slow growth rates (Fig. 1(c)), while the lower end of the bubble tends to remain higher (Fig. 1(d)). This behavior leads to bursting of the bubble at smaller size and lower He content, as shown in Fig. 1 (e). This is also reflected in the number of vacancies at the bursting point (see Fig. 1 (f)). Interestingly, we find that the nucleation of the first Frenkel pairs itself is isotropic for all growth rates when the bubble's surface is sufficiently far from the W surface and in the absence of other interstitials around the bubble. The cause of the breaking of this isotropy therefore lies elsewhere.

To understand the origin of these effects, we next study the behavior of interstitials from Frenkel pairs nucleated around the He bubble. We find that at the slowest growth rates considered in this work, the W interstitials, which

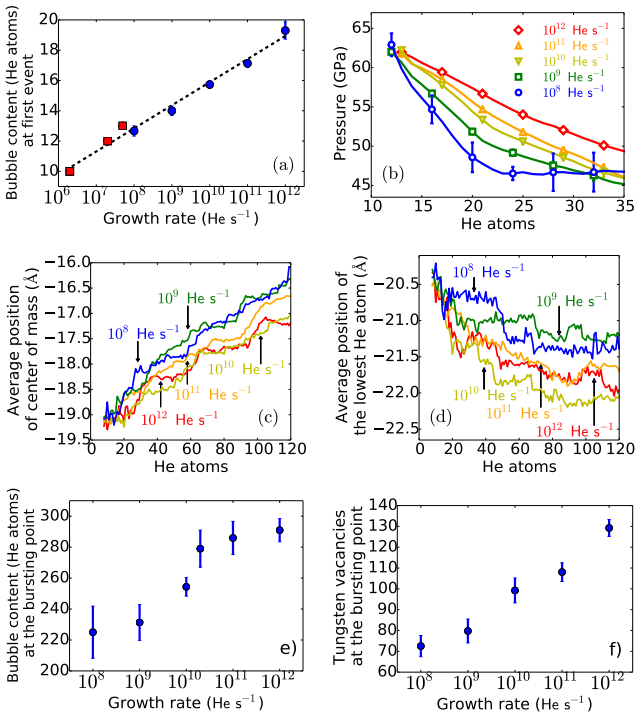

FIG. 1. Growth rate dependence of bubble growth. a) Average He content in the bubble at the time of the first detected event. Points with no error bars (red) are obtained from a single simulation. Points corresponding to rates $\geq 10^{11}$ He s^{-1} were obtained via direct MD simulations. b) Average pressure in the He bubble vs He content and growth rate. The limited number of simulations for the slowest rates significantly affect the average for He content larger than 25 atoms (blue line). c) Average position of the center of mass of the He bubble. d) Average position of the deepest He atom. e) Average He content in the bubble at the bursting point as a function of growth rate. f) Average number of W vacancies at the bursting point as a function of growth rate.

take the form of crowdions, are able to diffuse around the surface of the bubble. In this process, the crowdions change their orientation to any of the equivalent $\langle 111 \rangle$ directions that are tangential to the bubble surface. In Fig. 2(a) we show the diffusion hopping time as a function of the number of He atoms per W vacancy for two bubble sizes: a small bubble located in two W vacancies, and a larger bubble with 71 He atoms located in a symmetric arrangement of 15 W vacancies (the first two neighbor shells of a bcc atom). For the small bubble, the diffusion hopping time increases (diffusion becomes slower) with the number of He atoms in the bubble. This is likely due to the change in the stress field around the overpressurized bubble, something which will be explored in a future work. For the larger bubble we investigated the nucleation of new Frenkel pairs and the formation of adatoms, by using 8 independent ParRep simulations. Fig. 2(b) shows snapshots from a typical ParRep trajectory. After a period in which the interstitial diffuses around the

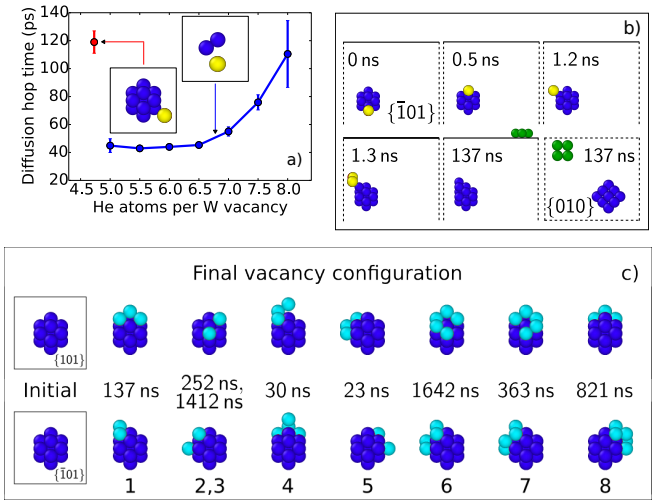

FIG. 2. a) Diffusion hopping time as a function of the number of He atoms per W vacancy for two cases: one W interstitial on a 2-vacancy bubble, and one W interstitial on a 15-vacancy bubble. Insets: red and blue spheres denote the W interstitial and W vacancies, respectively. b) Snapshots showing the diffusion of a W interstitial to the top of the bubble, the subsequent nucleation of additional Frenkel pairs, and the tearing off process of adatom nucleation. Green spheres denote adatoms on the W surface. c) Final vacancy configuration for the 15-vacancy bubble (after adatoms are formed) from 8 independent ParRep simulations. The orange spheres indicate the position of the additional vacancies. Top and bottom snapshots correspond to views on the planes {101} and {$\bar{1}$01}, respectively.

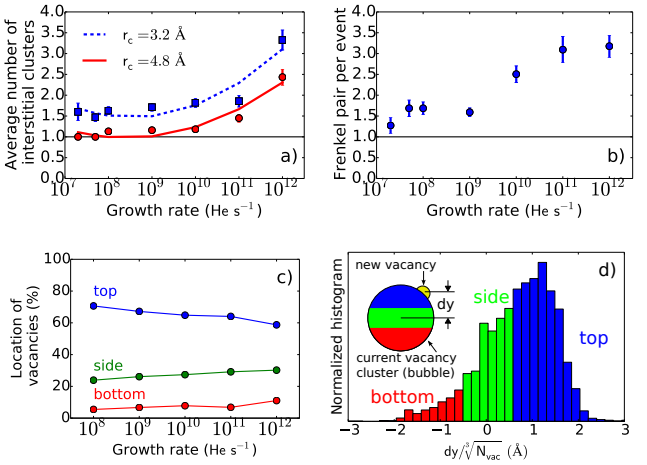

FIG. 3. a) Average number of interstitial clusters around the He bubble after a new Frenkel pair is nucleated, when at least one interstitial is already present, as a function of the growth rate, for two values of the cutoff distance defining the clusters. b) Average number of Frenkel pairs per event as a function of the growth rate. c) Spatial probability for the nucleation of new vacancies with respect to the center of the current vacancy cluster (see d)), as a function of the growth rate. d) Histogram of the location of new vacancies in the direction perpendicular to the surface for all the simulations. As described in the inset, the location is defined as the distance between the new vacancy and the center of the current vacancy cluster, binned into $dy = 1$ Å bins. In order to compare bubbles with different sizes this distance has been normalized by $\sqrt[3]{N_{vac}}$, with N_{vac} the number of vacancies already existing in the bubble.

surface of the bubble, new Frenkel pairs are nucleated at the top of the bubble, in the location of the first interstitial. Eventually, these "tear off", forming an island on the surface. The final vacancy arrangements for all the ParRep simulations are shown in Fig. 2(c), where the time needed to reach the corresponding configuration is also indicated. As in the case shown in Fig. 2(b), the new vacancies are typically nucleated at or near the top of the bubble and near existing interstitials; this corresponds to the growth of a dislocation line attached to the bubble surface. This process eventually leads to the formation of a complete loop which breaks away from the bubble, leading to the directed growth of the bubble towards the surface.

In light of these results, we can define a criterion to separate the fast and slow growth rate regimes: for a given bubble size, if the growth rate allows free diffusion of interstitials around the bubble on the timescale of He insertion, this corresponds to a slow growth regime with directed growth towards the surface. In contrast, for fast growth, the insertion rate of He atoms into the bubble is faster than this diffusion rate, so that the crowdion clusters associated with the interstitials (or the corresponding dislocation lines) grow faster than they can diffuse, leading to more isotropic growth of the bubble.

The results in Fig. 2(c) clearly show that subsequent nucleation of Frenkel pairs is biased towards the top of the bubble. To understand the mechanism causing this behavior, we examine the nucleation process of these Frenkel pairs in more detail. In Fig. 3(a), we plot the average number of distinct interstitial clusters around the He bubble just after a new Frenkel pair is nucleated in the presence of at least one other interstitial. The results show that, at slow growth rates, the nucleation of new Frenkel pairs preferentially occurs in the neighborhood of existing interstitials; that is, most of the time, the new interstitial contributes to the growth of an existing interstitial cluster (dislocation line); hence the number of interstitial clusters remains at about 1. In contrast, at fast growth rates, these nucleation events are less spatially correlated and new interstitial clusters are often created. Additionally, the number of Frenkel pairs nucleated in a single event depends on the growth rate, as shown in Fig. 3(b). On average, at fast growth rates the bubble grows via large steps involving many Frenkel pairs, while slow rates are characterized by small steps involving just one or two Frenkel pairs per event.

Further, as suggested by Fig. 2(c), these new Frenkel

pairs are not evenly distributed on the surface of the bubble. In Fig. 3(c) we show, as a function of the growth rate, the percentage of vacancies nucleated at the top, side and bottom of the bubble, until the bursting event, determined as illustrated in Fig. 3(d). The results show a favored growth of the bubble towards the surface at slow growth rates, while fast growth rates present a more isotropic growth.

Taken together, these results provide the following picture of the He bubble growth process under realistic (slow) growth rates. The first step is the isotropic nucleation of an initial W Frenkel pair on the surface of a bubble with no other W interstitials attached (Fig. 1(a)). The corresponding vacancy increases the bubble volume, while the interstitial becomes part of a $\langle 111 \rangle$ crowdion tangent to the bubble (Fig. 2). The interstitial diffuses around the bubble, a process that is faster for bubbles with less pressure (Fig. 2(a)). After more He atoms have entered the bubble, the bubble is able to drive the nucleation of another Frenkel pair, most likely in the neighborhood of the previous interstitial (Fig. 3(a)). Together, they form an incipient $\langle 111 \rangle$ dislocation line (arc). As it grows, the dislocation line interacts increasingly strongly with the surface, leading to its alignment towards it [26–28]. Eventually, this attraction drives an increase in the length of the dislocation line through the nucleation of more Frenkel pairs, preferentially from the top of the bubble because the interaction with the surface is there stronger (Fig. 3(c-d)). The arc then detaches, forming a $\langle 111 \rangle$ dislocation loop, which glides to the surface and creates an adatom island, increasing surface roughening (Fig. 2(b)). This directed growth towards the W surface leads to early bursting (Fig. 1(e)). The diffusion of the W interstitial around the bubble is the key mechanism that facilitates the localization of crowdions, and the subsequent nucleation of Frenkel pairs, on the top of the bubble. In contrast, at fast growth rates, either interstitial clusters grow where they are first nucleated or new Frenkel pairs are nucleated isotropically around the surface of the bubble. This leads to a more isotropic growth, delaying the bursting point as compared to the slow growth regime (Fig. 1(e)), and causing more surface damage because of the greater number of adatoms generated and the larger cavity left behind after bursting. Note that, as the bubble further approaches the surface, the nucleation of an isolated interstitial can itself be biased towards the top.

As mentioned in the introduction, a major issue with the use of W as a PFM is the formation of fuzz. Recently, a model of fuzz growth has been proposed that has at its core the balance between interstitial loop punching and bubble rupture [29]. This model captures the qualitative fuzz growth behavior and certain quantitative aspects, such as the fuzz thickness growing as $\sqrt{t}$. Central to the model are a number of assumptions, based on MD simulations, particularly that bubbles closer to the surface than a threshold distance, which depends on bubble radius, will rupture. In particular, the model assumes bubbles grow spherically, regardless of growth rate or proximity to a surface. Our results show that, especially at slower rates, bubbles near a surface, such as those that would be present in the fuzz filaments, grow anisotropically and their size at bursting will be much smaller than if they grew spherically. Further, our results indicate that the evolution of the surface morphology is very sensitive to how the bubbles grow, as where the interstitials are emitted from the surface of the bubble changes with the bubble growth rate. More generally, they highlight that the artificially fast growth rate in MD simulations can lead to an underestimation of the effect of the bias induced by the elastic interaction of the interstitials with different microstructural features (e.g. neighboring bubbles or dislocations) on the evolution of the system.

In conclusion, we have examined the growth of He bubbles in W for growth rates spanning six orders of magnitude using MD and ParRep. We find that there are two growth regimes, governed by the mobility of interstitials on the bubble surface. For slow He intake rates, bubble growth occurs at lower pressure, and is biased towards the surface, leading to early bursting. In contrast, at fast rates, growth occurs at high pressure, and proceeds more isotropically. These findings highlight the importance of simulating materials under realistic conditions, which could be an essential requirement to understand the fuzz formation.

The authors would like to thank Chun-Yaung (Albert) Lu for the useful discussion. LS, DP, and BPU acknowledge support by the U.S.DOE, Office of Science, Office of Fusion Energy Sciences and Office of Advanced Scientific Computing Research through the Scientific Discovery through Advanced Computing (SciDAC) project on Plasma-Surface Interactions. AFV was supported by the U.S. U.S.DOE, Office of Basic Energy Sciences, Materials Sciences and Engineering Division. This research used resources of the National Energy Research Scientific Computing Center, which is supported by the Office of Science of the U.S.DOE under Contract No. DE-AC02-05CH11231, and resources of the Oak Ridge Leadership Computing Facility at Oak Ridge National Laboratory, which is supported by the Office of Science of the U.S.DOE under Contract DE-AC05-00OR22725. Los Alamos National Laboratory is operated by Los Alamos National Security, LLC, for the National Nuclear Security Administration of the U.S. DOE, under contract DE-AC52-O6NA25396.

[1] D. M. Duffy, Mater. Today **12**, 38 (2009).
[2] S. J. Zinkle and L. L. Snead, Annu. Rev. Mater. Res. **44**, 241 (2014).

[3] G. Pintsuk, in *Comprehensive Nuclear Materials*, edited by R. Konings (Elsevier, 2012) p. 551.
[4] H. Iwakiri, K. Yasunaga, K. Morishita, and N. Yoshida, J. Nucl. Mater. **283-287**, 1134 (2000).
[5] M. J. Baldwin and R. P. Doerner, Nucl. Fusion **48**, 35001 (2008).
[6] M. J. Baldwin and R. P. Doerner, J. Nucl. Mater. **404**, 165 (2010).
[7] K. Henriksson, K. Nordlund, A. Krasheninnikov, and J. Keinonen, Appl. Phys. Lett. **87**, 163113 (2005).
[8] K. Henriksson, K. Nordlund, A. Krasheninnikov, and J. Keinonen, Fusion Sci. Technol. **50**, 43 (2006).
[9] M. Li, J. Wang, and Q. Hou, J. Nucl. Mater. **423**, 22 (2012).
[10] A. Lasa, K. Henriksson, and K. Nordlund, Nucl. Instrum. Meth. B **303**, 156 (2013).
[11] N. Juslin and B. D. Wirth, J. Nucl. Mater. **432**, 61 (2013).
[12] N. Juslin and B. D. Wirth, J. Nucl. Mater. **438**, S1221 (2013).
[13] F. Sefta, K. D. Hammond, N. Juslin, and B. D. Wirth, Nucl. Fusion **53**, 073015 (2013).
[14] F. Sefta, N. Juslin, K. D. Hammond, and B. D. Wirth, J. Nucl. Mater. **438**, S493 (2013).
[15] D. Nishijima, M. Miyamoto, H. Iwakiri, M. Ye, N. Ohno, K. Tokunaga, N. Yoshida, and S. Takamura, Mater. Trans. **46**, 561 (2005).
[16] A. F. Voter, Phys. Rev. B **57**, R13985 (1998).
[17] D. Perez, B. P. Uberuaga, and A. F. Voter, Comp. Mat. Sci. , (2015).
[18] S. Plimpton, J. Comp. Phys. **117**, 1 (1995).
[19] G. J. Ackland and R. Thetford, Phil. Mag. A **56**, 15 (1987).
[20] See Supplementary Material, which includes Refs. [30-39].
[21] D. E. Beck, Mol. Phys. **15**, 332 (1986).
[22] K. Morishita, R. Sugano, B. D. Wirth, and T. Díaz de la Rubia, Nucl. Instrum. Meth. B **202**, 76 (2003).
[23] W. D. Wilson, C. L. Bisson, and M. I. Baskes, Phys. Rev.B **24**, 5616 (1981).
[24] G. De Temmerman, K. Bystrov, R. P. Doerner, L. Marot, G. M. Wright, K. B. Woller, and D. G. Whyte, J. Nucl. Mater. **438**, S78 (2013).
[25] J. H. Evans, A. van Veen, and L. M. Caspers, Scr. Metall. **15**, 323 (1981).
[26] J. Baštecká, Cechoslovackij fiziceskij zurnal B **14**, 430 (1964).
[27] P. P. Groves and D. J. Bacon, Philos. Mag. **22**, 83 (1970).
[28] S. M. Ohr, J. Appl. Phys. **49**, 4953 (1978).
[29] A. Lasa, S. K. Tähtinen, and K. Nordlund, Europhys. Lett. **25002**, 105 (2014).
[30] S. Kajita, W. Sakaguchi, N. Ohno, N. Yoshida, and T. Saeki, Nucl. Fusion **49**, 95005 (2009).
[31] V. Borovikov, A. F. Voter, and X.-Z. Tang, J. Nucl. Mater. **254**, 447 (2014).
[32] C. H. Rycroft, G. S. Grest, J. W. Landry, and M. Z. Bazant, Phys. Rev. E **74**, 021306 (2006).
[33] "Visit," `https://wci.llnl.gov/codes/visit/home.html`.
[34] A. Stukowski, Modelling Simul. Mater. Sci. Eng. **18**, 015012 (2010).
[35] K. Nordlund, M. Ghaly, R. S. Averback, M. Caturla, T. Diaz de la Rubia, and J. Tarus, Phys. Rev. B **57**, 7556 (1998).
[36] L. Malerba, D. Terentyev, P. Olsson, R. Chakarova, and J. Wallenius, J. Nucl. Mater. **329-333**, 1156 (2004).
[37] A. F. Voter, F. Montalenti, and T. Germann, Annu. Rev. Mater. Res. **32**, 321 (2002).
[38] F. Sefta, N. Juslin, and B. D. Wirth, J. Appl. Phys. **114**, 243518 (2013).
[39] B. D. Wirth, Private communication.